Icarus **147**, 498–519 (2000)
doi:10.1006/icar.2000.6453, available online at http://www.idealibrary.com on IDEAL®

Instrument Calibrations and Data Analysis Procedures for the *NEAR* X-Ray Spectrometer

R. Starr, P. E. Clark, and M. E. Murphy

Physics Department, Catholic University of America, Washington, DC 20064
E-mail: richard.starr@gsfc.nasa.gov

S. R. Floyd, T. P. McClanahan, L. R. Nittler, and J. I. Trombka

Laboratory for Extraterrestrial Physics, NASA/GSFC, Greenbelt, Maryland 20771

L. G. Evans

Science Programs, Computer Sciences Corporation, Laurel, Maryland 20707

W. V. Boynton, S. H. Bailey, J. Bhangoo, and I. Mikheeva

Lunar and Planetary Laboratory, University of Arizona, Tucson, Arizona 85721

J. Brückner

Max-Planck-Institut für Chemie, Mainz, Germany

S. W. Squyres and E. M. McCartney

Astronomy Department, Cornell University, Ithaca, New York 14853

and

J. O. Goldsten and R. L. McNutt, Jr.

Johns Hopkins University, Applied Physics Laboratory, Laurel, Maryland 20723

Received December 10, 1999; revised May 30, 2000

The X-Ray spectrometer onboard the *Near Earth Asteroid Rendezvous* spacecraft will measure X-rays from the surface of 433 Eros in the energy region 0.7–10 keV. Detection of characteristic Kα line emissions from Mg, Al, Si, Ca, Ti, and Fe will allow the determination of surface abundances of these geologically important elements. Spatial resolution as fine as 3 km will be possible for those elements where counting statistics are not a limiting factor. These measurements will make it possible to relate Eros to known classes of meteorites and reveal geological processes that occurred on Eros. The calibration measurements and analysis procedures presented here are necessary for the reduction and analysis of the X-ray data to be collected during one year of orbital operations at Eros.

Key Words: **asteroids; instrumentation; X-rays; *NEAR*.**

INTRODUCTION

The *Near Earth Asteroid Rendezvous* mission (*NEAR*) was successfully launched on 17 February 1996. *NEAR* was the first launch under NASA's Discovery Program, an initiative for small, low-cost planetary missions. As the first spacecraft to orbit an asteroid, the *NEAR* mission will address fundamental questions about the processes and conditions relevant to planetary formation.

The X-ray/gamma-ray spectrometer (XGRS) is one of several instruments onboard the *NEAR* spacecraft that will study Eros during one year of orbital operations beginning in February 2000. The X-ray and gamma-ray spectrometers that compose the XGRS are independent, but complementary experiments. In this paper we focus on the X-ray spectrometer, its calibration,

0019-1035/00 $35.00

operation, and procedures for interpretation of the measurements to be made at Eros.

The X-ray spectrometer (XRS) will measure characteristic X-ray emissions induced in the surface of the asteroid by the incident solar flux. The Kα lines for the elements Mg, Al, Si, Ca, Ti, and Fe will be detected with spatial resolution on the order of 3 km when counting statistics are not a limiting factor. These measurements can be used to obtain both qualitative and quantitative information on elemental composition.

The X-ray spectrometer on the *NEAR* mission is a nondispersive spectroscopic system. In this approach, the incoming X-ray photon is absorbed by the detector material and a signal proportional to the absorbed energy is measured by the detector as a voltage pulse at the detector output. An analog-to-digital conversion is then performed and the count is binned by "pulse height" or energy loss, and a spectrum is obtained and telemetered to Earth. From an analysis of the pulse height spectrum, elemental composition can be inferred.

The choice among various types of X-ray detectors was strongly influenced by the constraints of the NEAR mission. The detectors were chosen for their sensitivity in the energy region of scientific interest, while also being consistent with the cost, mass, power, and reliability constraints of the mission.

X-RAY REMOTE SENSING

The most prominent fluorescent lines for the major elements Mg, Al, Si, Ca, Ti, and Fe are the Kα lines (1–10 keV). The strength of these emissions from planetary surfaces is strongly dependent on the chemical composition of the surface as well as on the incident solar spectrum, but is of sufficient intensity to allow orbital measurement by detectors like those on the *NEAR* spacecraft.

In addition to line fluorescence, solar X-rays also can be coherently and incoherently scattered from a planetary surface, contributing an unwanted background signal. Astronomical X-ray sky sources, which could be sources of background, are eliminated at Eros, because the XRS is collimated to a 5° field of view, and the asteroid completely fills the field of view when the spacecraft is below 100-km altitude.

The solar flux from 1 to 10 keV, the energy region of interest, can be modeled with several prominent lines superposed on a continuum described by a fourth- to sixth-order power law (depending on the level of solar activity). In modeling the solar output for the *NEAR* mission the best estimates of solar output anticipated near solar maximum have been used and range from approximately B1 to M1 levels. The solar intensity decreases by three to four orders of magnitude from 1 to 10 keV. Fluorescent lines as well as the scatter-induced background, therefore, have greater intensity at lower energies. As the level of solar activity increases, relatively more output occurs at higher energies, the slope of the spectrum becomes less steep, and the overall magnitude of the X-ray flux increases. This process is called hardening. Solar output is highly variable and can typically change by an order of magnitude or more within minutes. Higher solar activity will yield better statistics, shorter integration times, and hence higher resolution maps, especially for heavier elements such as Fe. Because of its variability, the Sun's output must be monitored in order to be able to obtain quantitative results. An introduction to X-ray remote sensing techniques for geochemical analysis can be found in Yin *et al.* (1993).

INSTRUMENT DESCRIPTION

Detectors

The asteroid-pointing detector package includes three large-area (25-cm^2) sealed gas proportional counters with thin (25-μm) Be windows. The large area provides the necessary sensitivity to achieve the desired spatial resolution and the Be windows absorb the lower energy X-rays (below 1 keV) that would otherwise dominate the detector count rate. The fill gas is P-10 (90% argon and 10% methane). The Be window is supported by a rectangular Be support structure. The detector housing is steel with a Be liner to absorb Fe line emission from the housing (Goldsten *et al.* 1997).

The sealed gas proportional counters chosen for this experiment are improved versions of instruments previously flown on Apollo 15 and 16. The energy resolution of current gas proportional counters is improved over those of the Apollo days, but is still not sufficient to resolve the low-energy Mg, Al, and Si lines. As with the Apollo missions it is necessary to use balanced filters to resolve these closely spaced lines (Adler *et al.* 1972a,b,c). Two of the detectors have thin absorption filters, approximately 9 μm thick, mounted externally. A Mg filter on one detector attenuates the Al and Si lines, and an Al filter on the other detector attenuates the Si line. The very steep absorption edges of the filters make the separation of the lower energy lines possible. The third detector has no filter. The energy resolution of these detectors is about 14% at 5.9 keV (Trombka *et al.* 1997).

Two sunward-pointing X-ray detectors positioned on the forward deck of the spacecraft monitor the incident solar flux. The solar monitors experience very strong X-ray emissions directly from the Sun, especially during solar flares, so the active area for a solar monitor needs to be only about 1 mm^2. One monitor is a proportional counter identical to the three asteroid-pointing detectors, but with a specially designed graded shield that reduces its effective area to about 1 mm^2 (Clark *et al.* 1995). The other solar monitor is a small Si-PIN photodiode. This solid-state detector is mounted on a miniature thermoelectric cooler in a hermetic package 15 mm in diameter. A 76-μm-thick Be window rejects the intense solar flux below 1 keV. The Si-PIN solar monitor achieves an energy resolution of 600 eV at 5.9 keV.

During each integration period the XRS collects four 256-channel pulse height spectra: one for each of the three asteroid-

pointing detectors and one from either the proportional counter or the PIN solar monitor. The two solar monitors may both be powered on at the same time, but telemetry limitations forced a design that allows only one of the solar monitors to be pulse height analyzed at a time. Additional details of the detector design can be found in Goldsten *et al.* (1997).

Collimator

A collimator is used to restrict the X-ray spectrometer field of view to about 5°. In a 50-km orbit (on average about 40 km from the surface of the asteroid) this results in a spatial resolution of about 3 km. The collimator is also useful in reducing the cosmic X-ray background. The collimator uses a honeycomb design made of copper with 3% Be. The K, L, and M X-ray lines excited in the collimator by solar X-rays, cosmic rays, and asteroidal X-rays do not interfere with the surface line emissions.

Calibration Sources

Three Fe-55 sources, mounted on a calibration rod, can be rotated, one at a time, into the field of view of the three asteroid-pointing detectors to establish the energy calibration of the XRS. Knowledge of the energy calibration of the XRS and how it changes over time is necessary to sum spectra obtained over the same region of the asteroid, but collected at different times during the mission. The statistics in any one spectrum (typically about a 100-s accumulation) are insufficient to perform detailed analysis.

DETECTOR CALIBRATIONS

In order to interpret the data collected by the XRS, a detailed understanding of the detector response is vital. Efficiency and energy resolution as a function of energy, angular response, filter transmission as a function of energy, and rise-time rejection efficiency are most important.

Asteroid-Pointing Detectors

One advantage of using an older, but well-known detector technology is that the characteristics of the system have been extensively studied and are well understood. The efficiency and resolution of gas proportional counters like those on *NEAR* have been measured many times. A detailed description of the response of proportional counters can be found in Knoll (1989).

The gas proportional counters on *NEAR* have a chamber diameter of 42 mm and are filled with P-10 gas, a mixture of 90% argon and 10% methane, to an absolute pressure of 1200 mbar. The anode wire is gold-plated tungsten and has a diameter of 13 μm. Figure 1 displays the detector efficiency versus energy calculated for this type of detector. The sharp features in the response of the Mg- and Al-filtered detectors at 1.30 and 1.56 keV, respectively, are the filter K-edges. The very sharp feature seen in all three detectors at 3.20 keV is the K-edge in argon, the primary constituent of the proportional counter fill gas. This feature complicates the response of the proportional counters for energies above the absorption edge, because the resulting K X-ray, which is 2.97 keV for argon, may escape the detector. A corresponding escape peak will then appear in the spectrum that lies below the full-energy peak by an amount equal to this characteristic energy. This can be seen in Fig. 2, which is the response of the Mg-filtered proportional counter to an Fe-55 source which emits the Mn Kα and Kβ lines at 5.899 and 6.490 keV, respectively. The fit to the measured pulse height spectrum (solid line) requires four peaks (dashed lines); one for the Kα line, one for the Kβ line, and one for each of the two escape lines. The full energy peak for the Kα line is seen in channel 150.6. The corresponding escape peak is in channel 75.4. From the energy calibration provided in the table in the upper left-hand corner of Fig. 2, this implies an energy difference of 2.97 keV, as predicted.

The energy resolution of gas proportional counters varies inversely as the square root of the energy,

$$\Gamma = 2.35\left(\frac{W(F+b)}{E}\right)^{1/2},$$

where Γ is the full-width at half-maximum (FWHM) as a fraction of the X-ray energy, W is the energy required to create an ion pair, F is the Fano Factor, b is a parameter that characterizes the avalanche statistics, and E is the energy in keV. (See, for example, Knoll, 1989). This equation represents the statistical limit for a gas proportional counter, which is the best response one can expect. For P-10 these parameters are $W = 0.026$ keV/ion pair, $F = 0.17$, and $b = 0.50$. The above equation then becomes

$$\Gamma = 0.310E^{-1/2},$$

At 5.9 keV this would imply an energy resolution of 12.8% or 0.753 keV. The energy resolution at 5.9 keV for the Mg-filtered detector as shown in Fig. 2 is 0.824 keV, or about 14.0%, which is typical for all the proportional counters on *NEAR*. An increase of about 10% over the statistical limit is expected for these detectors due to electronic noise and nonuniformity of the anode wire.

The response of a proportional counter to six different X-ray lines is shown in Fig. 3. The pulse height spectra were generated by using an α particle excitation source on targets of Mg (1.254 keV), Al (1.487 keV), Si (1.740 keV), S (2.307 keV), Ca (3.690 keV), and Ti (4.508 keV). The fractional energy resolution of each of these six X-ray lines, plus the 5.899-keV line from Fe-55, is plotted versus energy in Fig. 4. The fitted line is a power-law function in energy with a slope of -0.5 and a constant of proportionality of 0.340. The energy resolution for Ca and Ti is 17.7 and 16.0%, respectively. The energy of the Fe Kα line

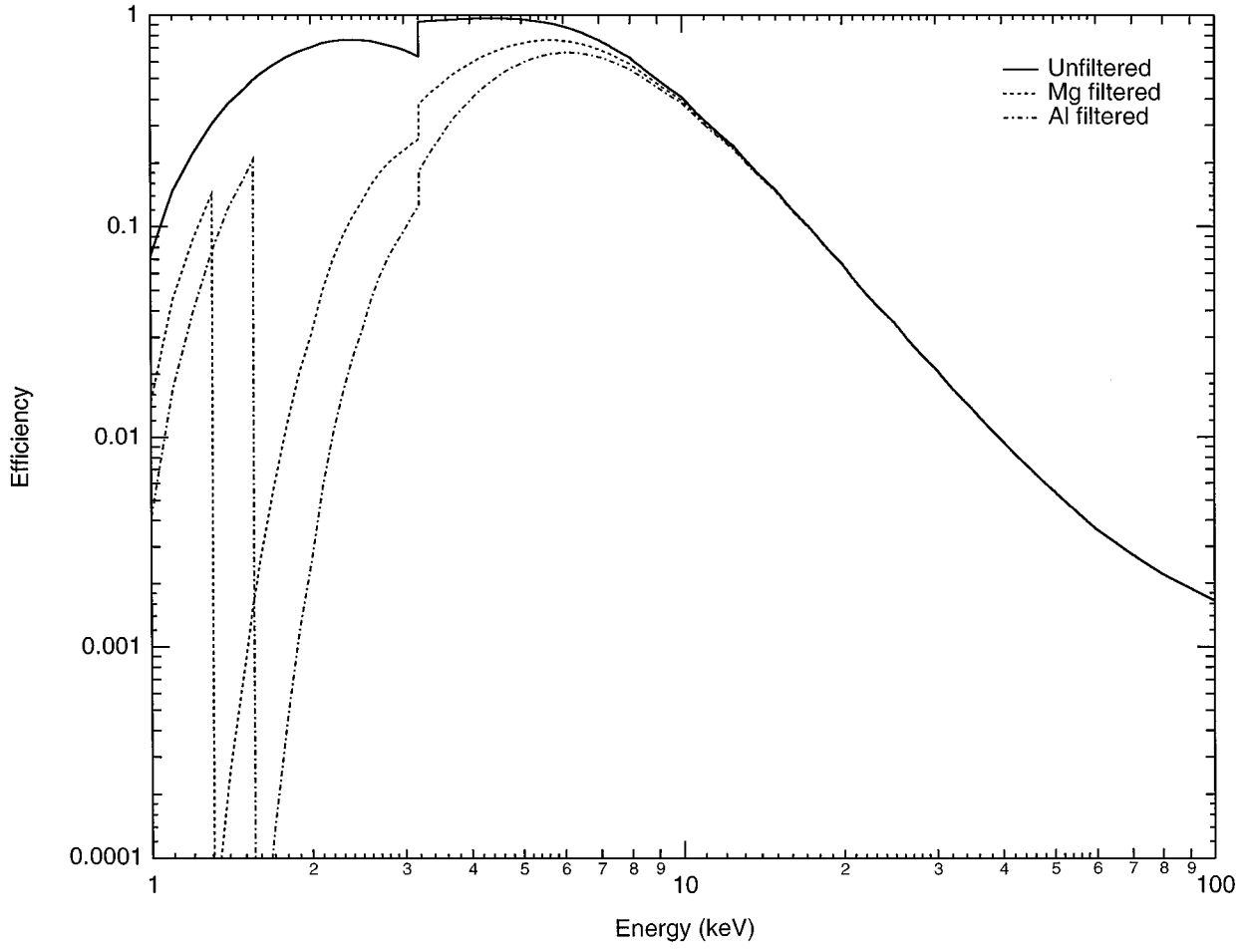

FIG. 1. Detector efficiency versus energy for *NEAR* XRS proportional counters. The effect of the Mg and Al filters at low energies is clearly seen. The break in the curve near 3.2 keV is the argon K-edge. The 25-μm-thick Be window attenuates the lower energy X-rays.

that will be emitted from the asteroid surface is 6.40 keV, and the resolution at this energy is 13.4%. While there will be some overlap of these lines in the spectra collected from the asteroid, the energy resolution of the proportional counters will still be sufficient to resolve them.

A collimated Fe-55 source, positioned in a plane perpendicular to the detector face, was used to map the response of the detector over the entire window area. This result is shown in Fig. 5. The FWHM of the detector response with the collimator in place is 3.2°. The full-width at tenth-maximum (FWTM) is 5.5°. The radial response of the detector is isotropic.

As described above, it is necessary to use thin filters in front of two of the three proportional counters in order to separate the three low-energy lines of Mg, Al, and Si. Figure 6 shows the response of the unfiltered, Mg-filtered, and Al-filtered gas proportional counters to these three X-ray lines. The Mg filter significantly reduces the Al and Si line intensities relative to the Mg line. The Al filter reduces the Si line intensity relative to the others. Using this method, the three overlapping lines of Mg, Al, and Si can be separated. The details of this technique for line separation are discussed later.

The effectiveness of the rise-time discrimination circuitry is displayed in Fig. 7. An in-flight spectrum taken with the Fe-55 calibration source in the detector field of view is shown. The rejection efficiency for gamma rays and charged particles was determined to be ~70% by comparing the background counts above channel 51 with and without rise-time discrimination enabled. A comparison of the counts in the Fe-55 peak shows that only about 5% of the Fe-55 X-rays are removed by the rise-time circuitry. Rise-time discrimination is disabled below about 2 keV (channel 51). Below this energy, the rise time of X-rays, gamma rays, and cosmic rays is not sufficiently different to allow efficient rejection of the background without loss of a significant amount of valid X-ray events.

Solar Monitors

The *NEAR* XRS has two solar monitors. One is a solid state Si-PIN diode, and the other is a gas proportional counter identical

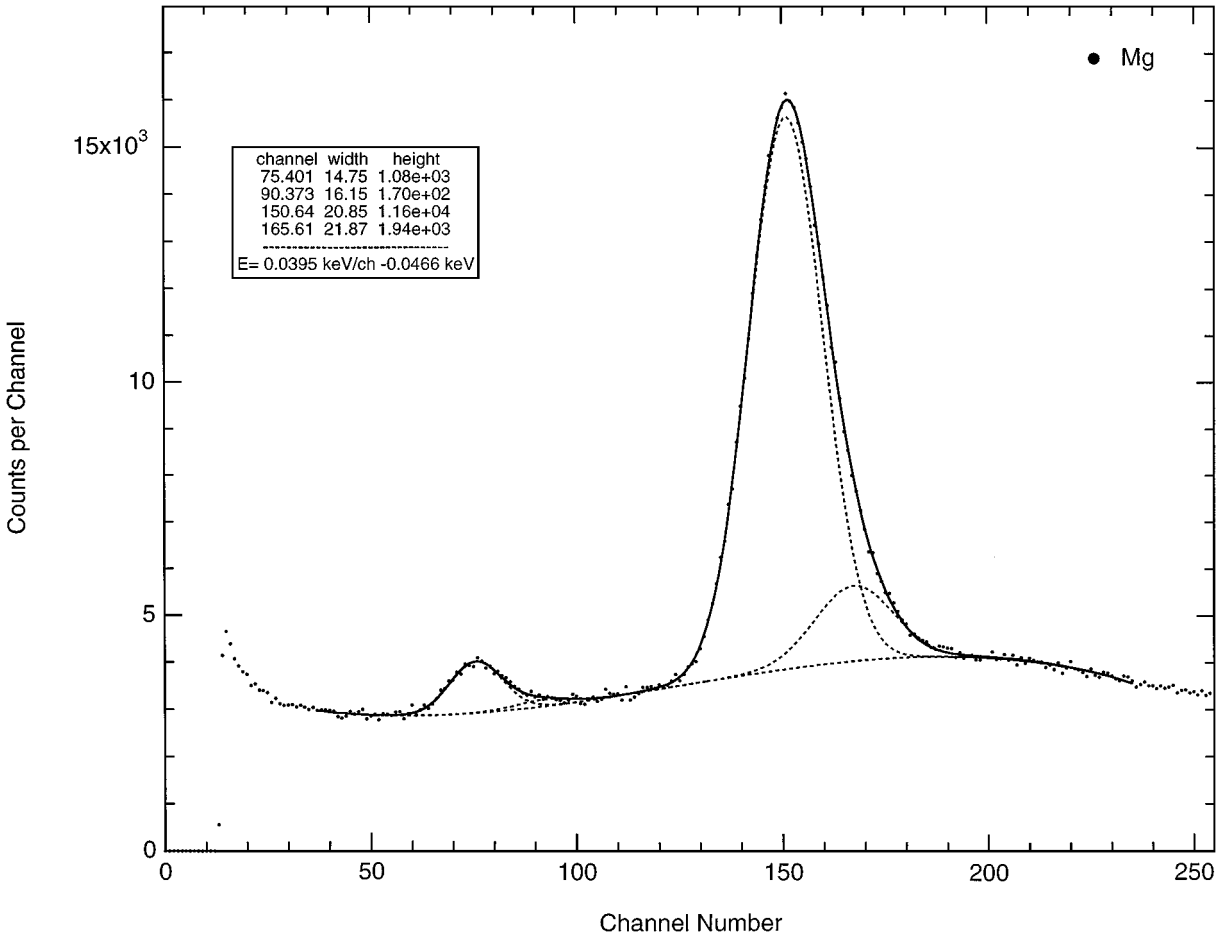

FIG. 2. Response of Mg-filtered proportional counter to an Fe-55 source. The fit to the spectrum (solid line) is accomplished by including the Kα (5.899 keV) and Kβ (6.490 keV) Mn lines in both the full energy and escape peaks (dashed lines) plus a polynomial for the background (dashed line). The fit for the full energy Kα line gives a FWHM of 824 eV.

to the three asteroid-pointing detectors, but with a specially designed graded shield. The gas proportional counter is the primary solar monitor. The PIN detector was added as an engineering test of this new technology. For the PIN detector the efficiency is easily calculated. It is a Si detector 300 μm thick with a 76-μm-thick Be window and a 200-nm dead layer. The result of this calculation is shown in Fig. 8. The impact of the Be window on the efficiency at low energies is evident. The efficiency of the Si-PIN detector at 5.9 keV was measured using an Fe-55 source of known strength, placed on axis at a fixed distance from the detector. The result was 0.95 ± 0.04, which is in good agreement with the calculated value of 0.96. The error reflects the statistical uncertainties, only.

Figure 9 is a pulse height spectrum of the Si-PIN with an Fe-55 source in the field of view. The Kα and Kβ lines merge, but are separated by the fit. The FWHM of the Kα line (5.9 keV) is 0.60 keV or 10.2%. Low-energy electronic noise is seen below channel 42 or about 1.7 keV.

As with the proportional counters, the energy resolution of the Si-PIN varies inversely as the square root of the energy. Using the measured resolution of 0.60 keV at 5.9 keV to determine the proportionality constant gives the FWHM as a fraction of the X-ray energy:

$$\Gamma = 0.247E^{-1/2}.$$

The gas proportional counter solar monitor is identical to the three asteroid-pointing detectors, but with the addition of a graded shield (Clark *et al.* 1995). This shield is designed to restrict the effective area of the detector to about 1 mm^2, and also to attenuate more of the lower energy flux from the Sun in order to enhance the response of the detector at the higher energies. The response of the gas solar monitor is shown in Fig. 10, along with that of a bare proportional counter and the Si-PIN diode. The effectiveness of the shield can be seen by the comparison of the two proportional counter response curves.

A comparison of solar spectra from the proportional counter and Si-PIN solar monitors is shown in Fig. 11. The solid traces are the gas proportional counter and the dashed traces are the

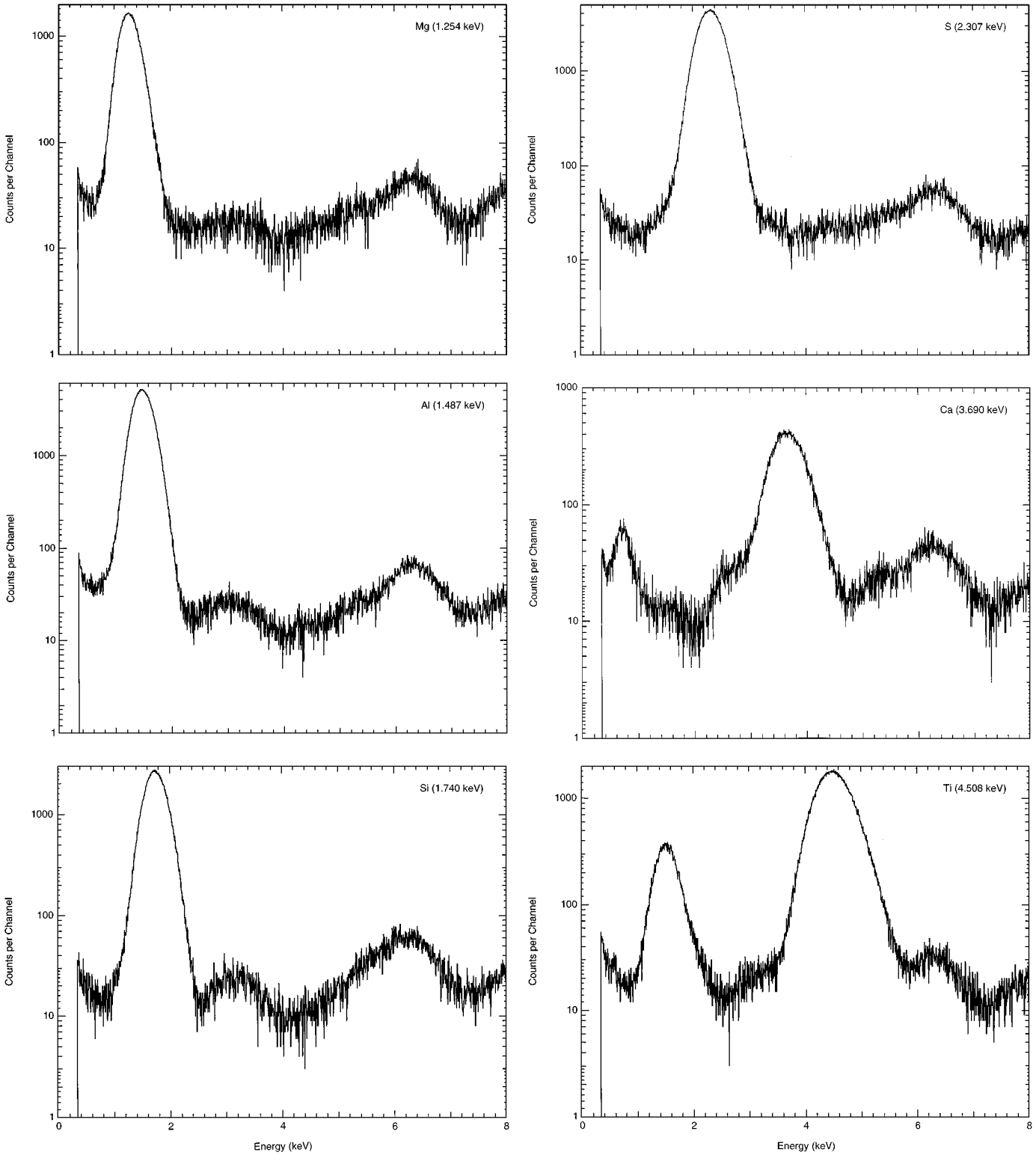

FIG. 3. Monoelemental pulse height spectra generated with an α particle source exciting targets of Mg, Al, Si, S, Ca, and Ti. Argon escape peaks for the Ca and Ti targets can be seen. The energy calibration used here corresponds to a channel width of 5.74 eV.

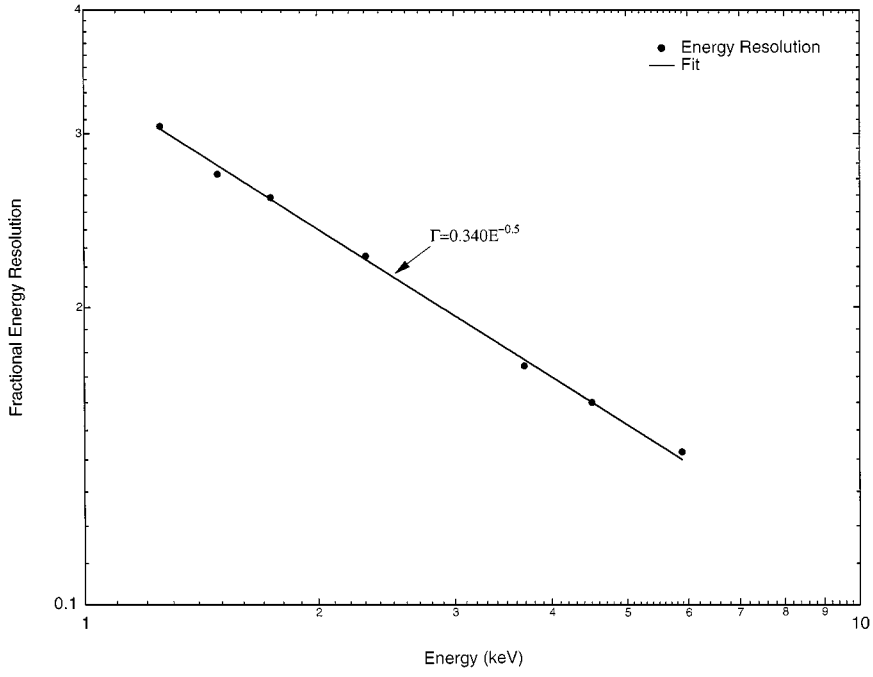

FIG. 4. The energy resolution of a gas proportional counter as a function of energy. The fit to the data points is a power law in energy and agrees well with the expected value.

Si-PIN detector. The lower two traces show spectra collected during a quiescent period. Note the significantly lower background in the solid-state detector. The upper two traces show spectra collected during a solar flare. The predominant line near channel 170 indicates strong Fe X-ray emissions (∼6.6 keV). The proportional counter spectrum clearly shows the effect of the graded shield in "hardening" the detector response to solar input. At low energies the response of the two detectors is nearly

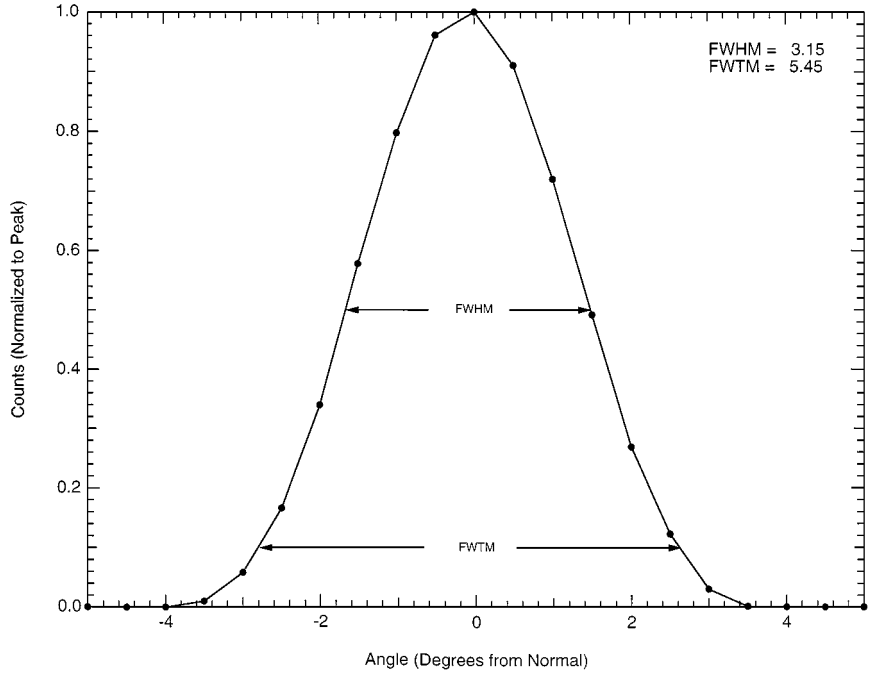

FIG. 5. Response of collimated gas proportional counter to an Fe-55 source located in a plane perpendicular to the detector face. The field of view of the detector is collimated to 3.2° FWHM and 5.5° FWTM. In the radial direction, the field of view is isotropic.

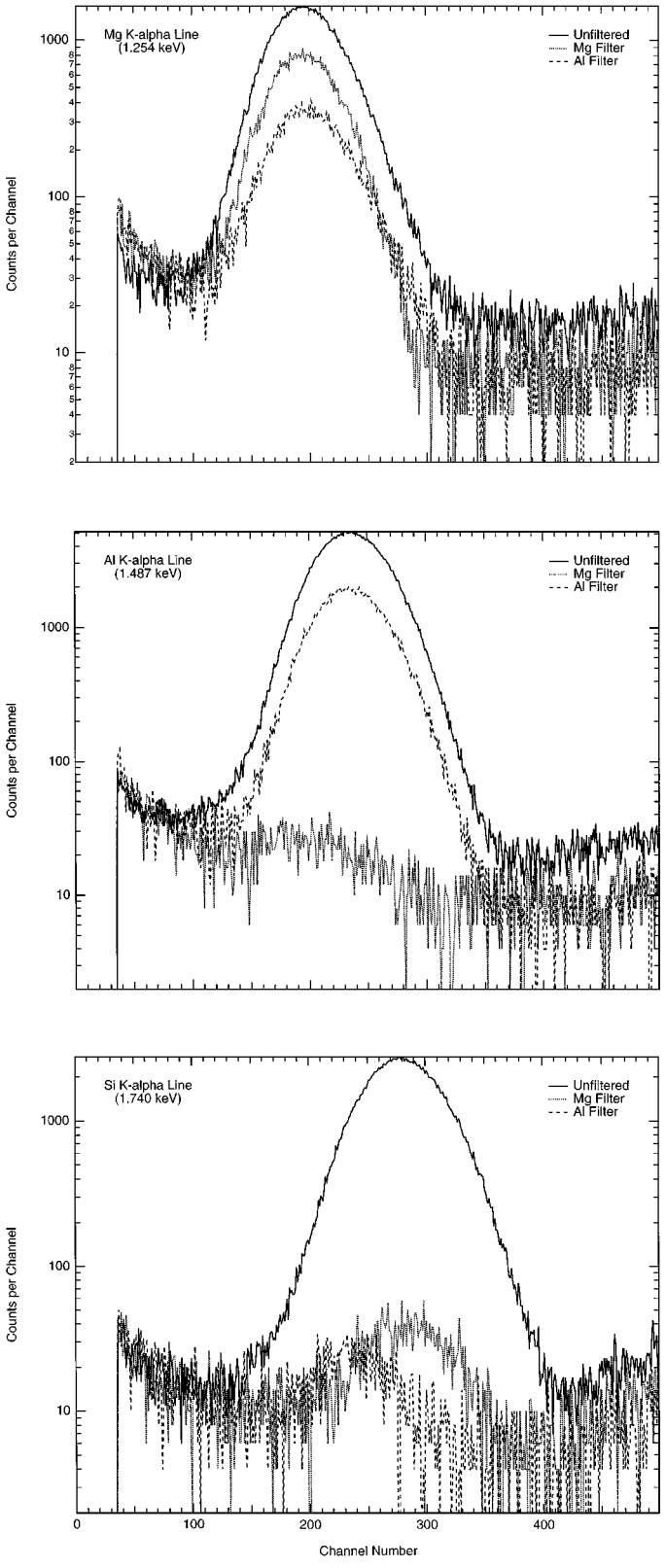

FIG. 6. Response of gas proportional counters to Mg (top), Al (middle), and Si (bottom) Kα X-ray lines. The effect of the Mg and Al filters is shown. The Al X-ray is effectively eliminated by the Mg filter, and the Si line is removed by both the Mg and Al filters.

the same, while at higher energies the gas solar monitor response is significantly greater than that of the Si-PIN.

INSTRUMENT OPERATION

Understanding how the XRS operates is essential to reducing and analyzing the data it returns and ultimately extracting the surface compositional information for Eros that is the goal of this mission. The following sections describe the more important operational considerations for the *NEAR* XRS.

High Voltage and Temperature Stability

The four XRS proportional counters each operate at voltages close to 1165 volts. The high voltage control circuitry maintains the voltage on the proportional counters to within about 0.5 V of the commanded value (Goldsten *et al.* 1997). This is important because small changes in high voltage can produce significant changes in detector gain. On the other hand, the proportional counters are relatively insensitive to temperature changes, so other than keep-alive heaters, no effort is made to control the temperature of the proportional counters. The result is that over several thousand hours of XRS operations during cruise, no significant gain changes have been observed due to voltage or temperature changes.

The bias voltage of the Si-PIN is 30 V. This voltage is controlled by the same circuitry as that used by the proportional counters. The Si-PIN must be cooled to temperatures below -20°C in order to operate properly. This is accomplished by the miniature thermoelectric cooler. The temperature is maintained within allowable limits by on-board control, and the gain of the Si-PIN has also been quite stable throughout cruise operations.

Energy Range

Each of the five XRS detectors generates a 256-channel pulse height spectrum. The nominal width of each channel is about 40 eV, giving an upper level energy of about 10 keV. The lower end of the energy range depends upon the setting of the lower level discriminators (LLD). For the proportional counters this is typically channel 15 which corresponds to $\sim$0.60 keV. For the Si-PIN the LLD is set to channel 37 because of electronic noise, so its pulse height spectrum measures down to about 1.5 keV.

Live Time

The live time of each of the five XRS detectors (including the nonactive solar monitor) is available with each science record. These are simply calculated from two counters associated with each of the detectors: valid rate and raw rate. The raw rate is every count registered in a detector above the lower level discriminator. The valid rate represents all counts processed by the XGRS digital processing unit (DPU). The ratio of valid to raw gives the live time.

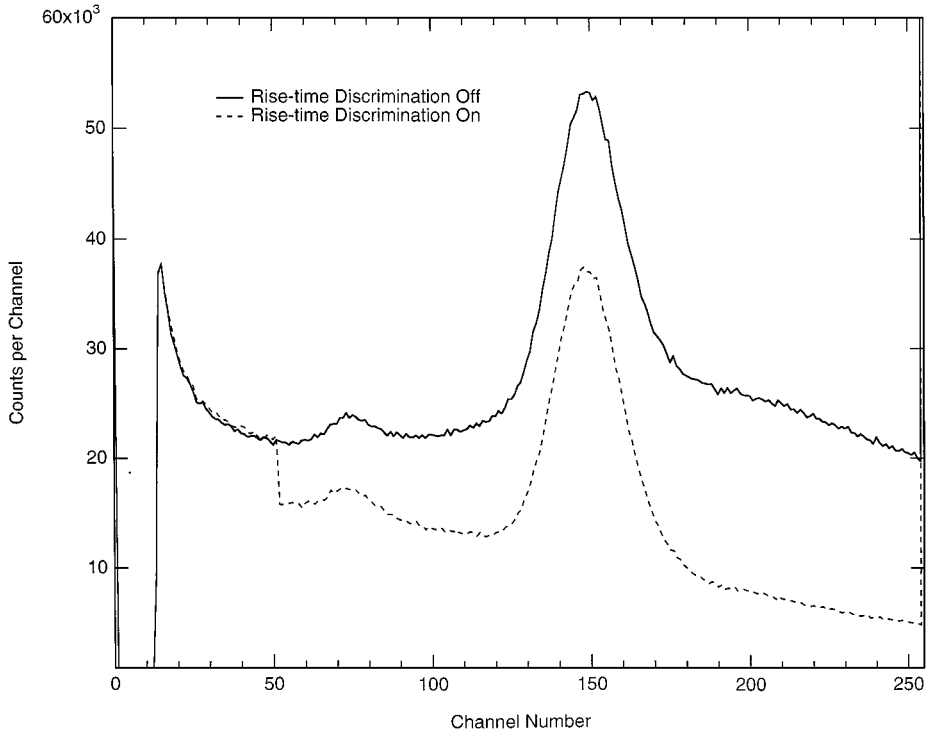

FIG. 7. Response of Al-filtered X-ray proportional counter to Fe-55 source. The solid curve is rise-time discrimination off and the dashed curve is rise-time discrimination on. The break in the dashed curve at channel 51 is the valid rise-time discriminator threshold.

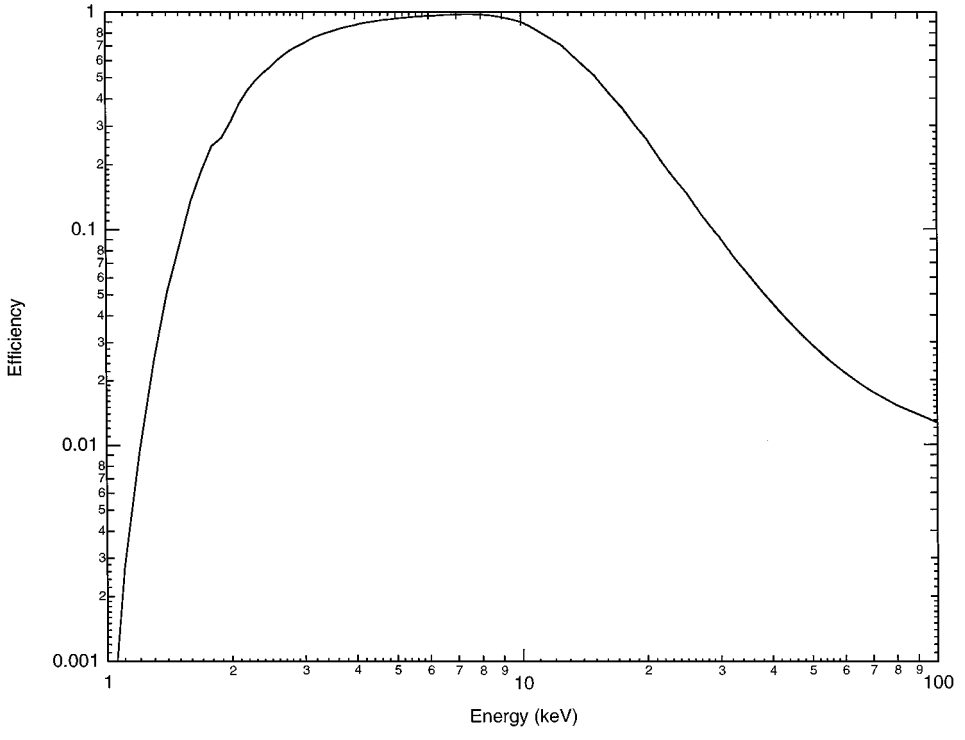

FIG. 8. Efficiency of Si-PIN detector versus energy. The 76-μm-thick Be window strongly attenuates the lower energy X-ray flux from the Sun that would otherwise dominate the detector.

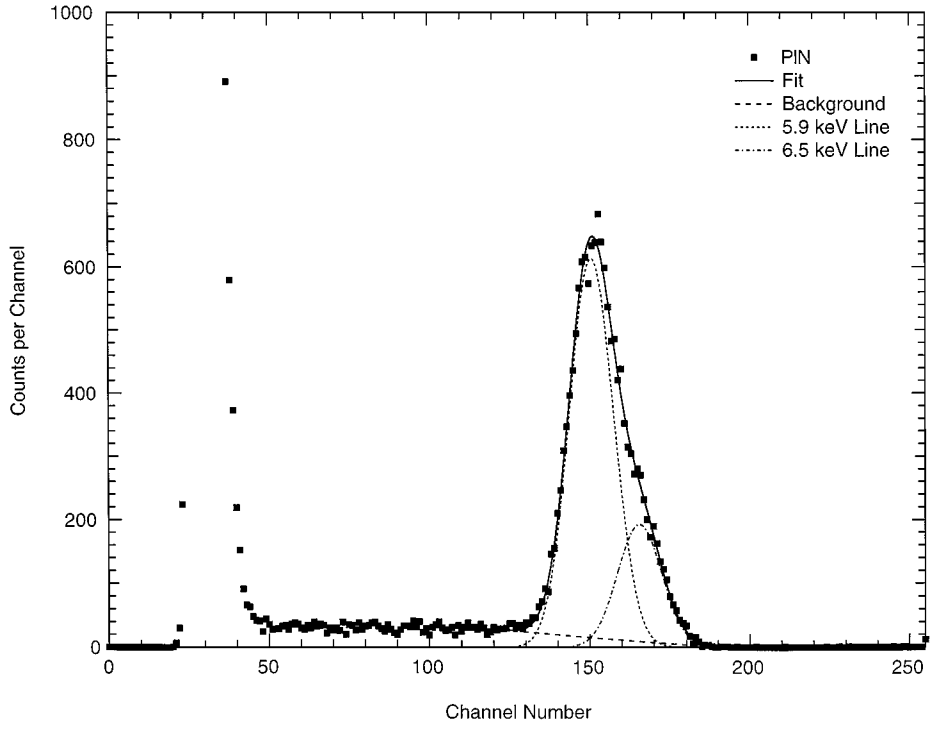

FIG. 9. Response of Si-PIN detector to an Fe-55 radioactive source. The Kα (5.90 keV) and Kβ (6.49 keV) lines overlap, but their separate contributions can be seen by the fit and its two components. The FWHM of the Kα line is 600 eV.

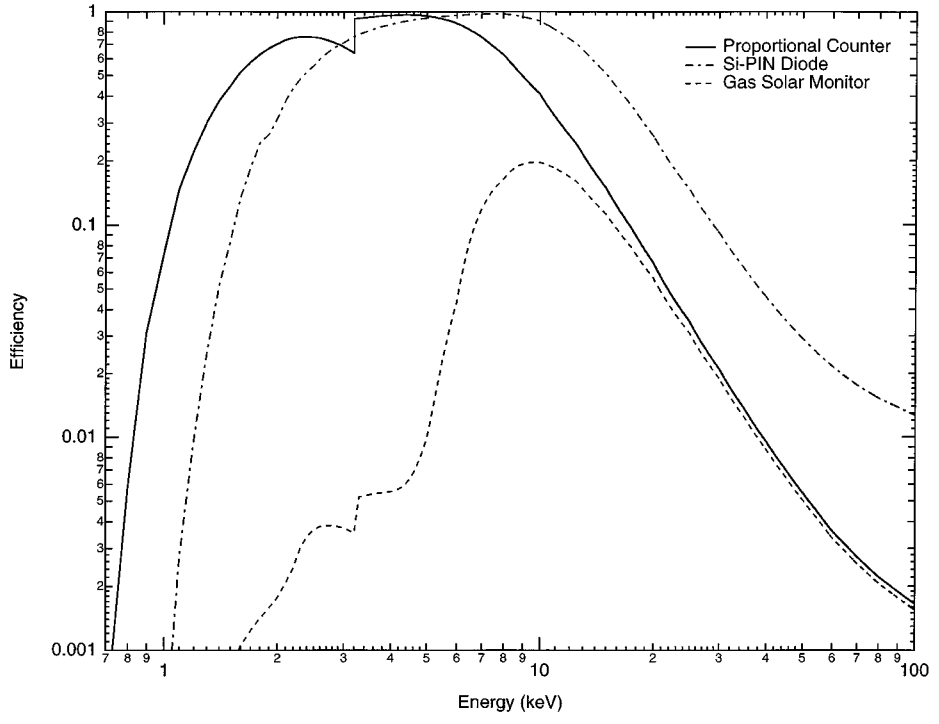

FIG. 10. Response of a bare proportional counter (no filter), PIN solar monitor, and gas proportional counter solar monitor. The curves for the proportional counter and PIN are the same as those in Figs. 1 and 8, respectively. The effect of the graded shield on the low-energy response of the gas solar monitor can be seen.

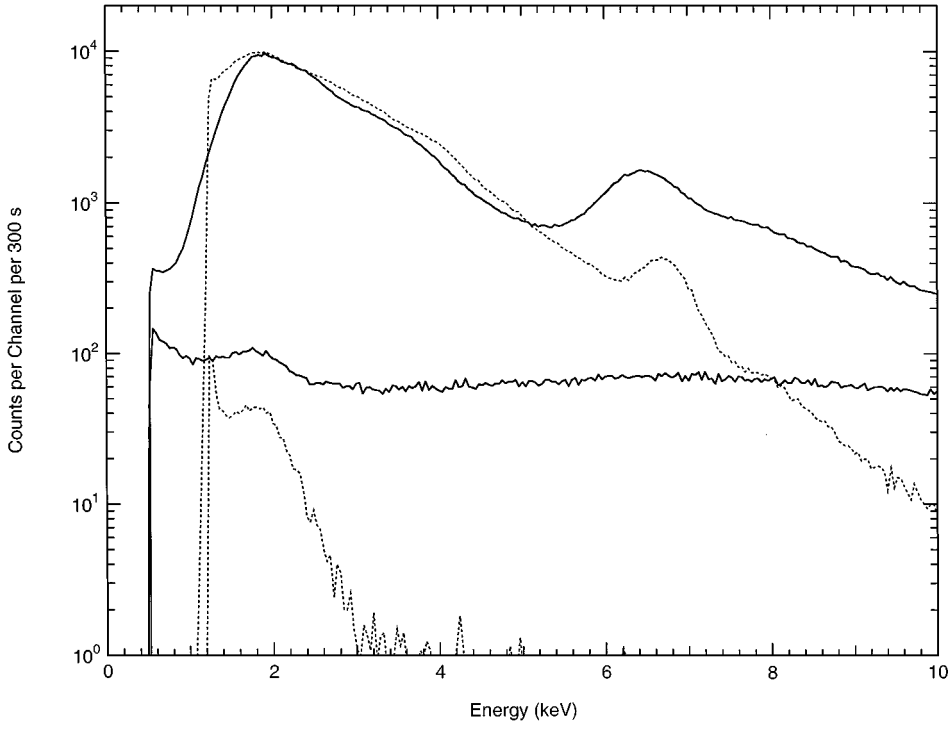

FIG. 11. A comparison of spectra collected in flight from the proportional counter and Si-PIN solar monitors. The solid traces are the gas proportional counter and the dashed traces are the Si-PIN detector. The lower two traces show spectra during a quiescent period (10 January 1998). Note the significantly lower background in the solid-state detector. The upper two traces show spectra during a solar flare (15 January 1998). The predominant line near 6.6 keV indicates strong Fe X-ray emissions. The proportional counter spectrum clearly shows the effect of the graded shield in flattening the detector response to solar input. All four spectra are normalized to 300-s accumulations and 1 AU.

One correction needs to be made to this simple relationship. When the bismuth-germanate (BGO) shield in the gamma-ray spectrometer detects a very high-energy cosmic ray its preamplifier saturates, which causes cross talk in the asteroid-pointing proportional counters. The spectra are not contaminated, because whenever a high-energy event is detected in the BGO, the X-ray channels of the three asteroid-pointing detectors are cleared, but the raw rate is a hardware counter and cannot be decrimented. A correction must be made to the raw rates using the cross-talk counter, which is one of the 41 rate counters available in the XRS science records. Based on laboratory and in-flight measurements, the following equations for live time are used for the three asteroid-pointing detectors:

$$\text{Unfiltered Detector Live Time} = \frac{\text{UNF\_VALID\_EVENTS}}{\text{UNF\_RAW\_EVENTS} - 0.037 \times \text{XTALK\_COUNTER}}$$

$$\text{Mg-Filtered Detector Live Time} = \frac{\text{MG\_VALID\_EVENTS}}{\text{MG\_RAW\_EVENTS} - 0.025 \times \text{XTALK\_COUNTER}}$$

$$\text{Al-Filtered Detector Live Time} = \frac{\text{AL\_VALID\_EVENTS}}{\text{AL\_RAW\_EVENTS} - 0.031 \times \text{XTALK\_COUNTER}}.$$

The two solar monitor detectors are unaffected by BGO saturation events because their preamplifiers are located on the opposite side of the spacecraft from the gamma-ray electronics. For these two detectors no cross-talk correction is necessary. Typical live times for the asteroid-pointing detectors are about 97%. The proportional counter solar monitor live time varies significantly with solar activity. During quiescent periods it is typically over 90%, but will drop below 60% during large flare events. The Si-PIN live time is generally higher than that of the proportional counter, usually better than 90% even during large flares. This difference is due to the very fast rise time of the electronic pulses in the Si-PIN.

Rise-Time Discrimination

The gas proportional counters are subject to a large number of background events from cosmic-ray and gamma-ray interactions in the detectors. Rise-time discrimination can be used to reduce this background component, because the rise time of the electronic pulses produced by the proportional counters due to these interactions is longer than that for X-rays. Rise-time discrimination circuitry employed on the XRS rejects up to 70% of these background events. The rise-time threshold can be adjusted by ground command. The nominal setting for all four proportional counters is 135, which corresponds to a rise-time threshold of 0.5 μs.

Below about 2 keV, pulse rise-time differences between the X-ray signal and the various background events are no longer large enough to be easily separated by the rise-time logic. As a result, it is necessary to disable rise-time discrimination below 2 keV in order to prevent the rise-time circuitry from discarding too many valid events. This, of course, results in much higher background in this energy region. This rise-time valid threshold can be adjusted by ground command for each of the gas proportional counters. Setting this threshold to 0 or 255 turns rise-time discrimination off for all channels. The nominal setting is channel 51 for the asteroid pointing detectors. The effect of rise-time discrimination can be seen in Fig. 7. The valid rise-time channel setting for the proportional counter solar monitor is 255. Rise-time discrimination is not routinely used on this counter since solar X-rays dominate even during solar quiescent periods and cosmic-ray background is not nearly as significant a factor as it is for the other proportional counters.

The Si-PIN is not subject to any of these high-energy background components because the energy deposited in the detector by a cosmic ray or gamma ray is much higher than the upper range for pulse height analysis—about 10 keV. No rise-time discrimination is used on the Si-PIN detector.

Instrument Safing

The X-ray detectors may be damaged by very high count rates. For this reason, flight software was designed to remove high voltage from any detector whose count rate exceeded a preset level. Normally, this level is 30,000 counts/s, but may be adjusted by ground command. If this threshold is exceeded, the high voltage is turned off for one hour (adjustable by ground command). After one hour the voltage is increased slowly (about 100 V every 20 s). If the count rate exceeds the safing threshold the high voltage is again reduced to zero. Up to six retries (adjustable by ground command) are attempted. After this, high voltage can be restored only by explicit ground command.

DATA REDUCTION AND ANALYSIS

Introduction

The XRS measurements must be corrected for a number of factors in order to determine the incident photon flux from the asteroid. Once the incident flux is determined, both qualitative and quantitative geochemical information can be inferred. In order to obtain elemental composition from the measured pulse height spectra, it is necessary to adjust the spectra to a common energy scale, normalize for solar activity, correct the spectrum for geometric factors (e.g., variations in altitude), correct for surface substrate matrix effects, and correct for the changing angles of incidence and emission. Finally, the individual spectra may be summed and background subtracted. At this point, it is then possible to convert the spectrum from pulse height to photon flux, and then from photon flux to elemental composition. Detailed discussions of these processes can be found in Clark (1979), Trombka *et al.* (1979), Yin *et al.* (1993), and Clark and Trombka (1997).

A shape model of the asteroid, developed using data from the *NEAR* imager (Veverka *et al.* 1997) and from the laser altimeter (Zuber *et al.* 1997), will be used to determine the accumulation regions (bins) on the asteroid. Bin sizes will be selected based on the instrument viewing footprints and integration times required to obtain statistically significant results. The incident solar X-ray spectrum is measured with the solar monitors and stored as part of each record. A correction is made for the variation in angle of incidence of the solar flux, and asteroid spectra are normalized by taking into account the shapes and intensities of the associated solar spectra. The local altitude is also stored with each spectrum, and solid angle corrections due to changes in altitude are determined. Once the various corrections have been applied to the spectra, they then can be summed. This basic procedure was developed for the analysis of the spectra obtained during the Apollo program and was used successfully (Trombka *et al.* 1979).

The X-ray background that is not rejected by the rise-time discrimination circuitry can be attributed to coherent scattering of solar and sky X-ray sources from the surface of the asteroid. The magnitude and shape of the sky component can be determined from measurements made on the dark side of the asteroid. During the Apollo missions, it was found that this component was constant, so that the dark-side background could be subtracted directly from the pulse height spectra measured on the sunlit side (Trombka *et al.* 1979).

For X-ray measurements, given a number of samples with the same elemental bulk composition, X-ray intensity will depend not only on the elemental composition, but also on the physical state of the sample material (e.g., particle size and distribution). This matrix effect is very similar for X-ray lines that are close in energy, so substrate matrix effects can be significantly reduced by taking line intensity ratios. These ratios also cancel out most other geometric factors, since they are only weakly energy and element dependent (Adler *et al.* 1972a,b,c).

Methods for performing transformations from pulse height to photon energy space have been developed for data from instruments similar to the *NEAR* XRS such as the Apollo X-ray spectrometer (Trombka *et al.* 1979). A number of methods may be used to perform these transformations including least-squares analysis, spline techniques, peak search, and simple matrix transformations. Several different methods will be used on the same spectra to confirm the analysis.

The final step in the data interpretation process is the inference of elemental composition from an analysis of the photon intensities detected in orbit. Laboratory and field calibrations, in conjunction with theoretical calculations, are required in order to obtain photon-to-elemental composition conversion factors. The approach developed for the analysis of the X-ray spectrometer data is described in Clark (1979) and Clark and Trombka (1997).

LEVEL 0 DATA PRODUCTS

The level 0 data products are just the raw data returned by the XRS. The XRS produces four X-ray spectra and 41 rate counters every integration period. All spectra contain 256 channels. Spectral bins contain 16 bits. Rate counters are 32 bits. The spectra correspond to the unfiltered proportional counter detector, the Mg-filtered detector, the Al-filtered detector, and the active solar monitor. Both solar monitors may be on at the same time, but spectra from only one of the solar monitors may be returned for any integration period. Rate counters include raw event rates and valid event rates for each of the five X-ray detectors. In addition, for the four proportional counters, rise-time reject, true rise-time reject, false rise-time reject, and cross-talk rates are also provided.

The X-ray data set also includes both science and engineering housekeeping. The science housekeeping data set contains 53 parameters and the engineering housekeeping data set contains 162 parameters. These two data sets contain the 41 rate counters as well as engineering information such as high voltage, lower level discriminator settings, temperatures, location of the Fe-55 calibration rod, and many other engineering parameters that allow the experimenters to evaluate the status of the instrument. A few of the more important housekeeping parameters are discussed below.

Mission Elapsed Time

Every science record returned by the XRS is time tagged with the spacecraft mission elapsed time (MET). Data processing uses MET to access the SPICE kernels to return positions of the Sun, Earth, and the spacecraft in the asteroid body fixed coordinate system. SPICE is a data system that contains the geometric and other ancillary information needed to correlate individual instrument data sets with data from other instruments, spacecraft ephemeris, attitude information, and other relevant geometric and timing parameters.

Data Quality Index

One of the parameters returned as part of the science housekeeping records is DQI or data quality index. This parameter is zero if all of the data packets for a science record have been received at the APL Science Data Center (SDC). DQI is set to one if any packets are missing.

Integration Time

The integration time of each spectrum is included with each science record. During orbit this time will most often be 100 s. There will be some cases when integration periods will be shorter. One example is if a command is sent to the XRS for immediate execution. So as not to corrupt the current record, the integration period is terminated prematurely, the command is executed, and a new 100-s integration period begins. Each of the four returned spectra has its own integration time that are normally the same, but in some unusual circumstances may differ. For example, each channel of the four 256-channel spectra is 16 bits. If the number of counts in any channel of a spectrum exceeds 65,535 during an integration period, accumulation stops for that one detector (though channel rollover and continued detector accumulation can be permitted by ground command). This has happened occasionally for the solar monitors during periods of intense solar activity. Count rates exceeding 30,000 per second will cause detectors to safe themselves as described earlier. Here again, the integration period will be terminated early. This too has been observed during cruise, usually for the solar monitors. They recover autonomously when the count rate drops below 30,000 per second.

LEVEL 1 DATA PRODUCTS

The level 1 data products are the raw data records with spectral gain corrections, spatial parameters, and other derived parameters added to each record. Beginning in February 2000, the *NEAR* spacecraft will spend about one year in orbit around 433 Eros. The XRS will accomplish most of its highest quality observations during the 175 days in low orbit—50 km or less. Assuming 100-s integration periods during most of this time implies 864 records per day and over 150,000 records for just the low-orbit portion of the mission. Each one of the science records returned by the XRS contains four 256-channel spectra, 53 science housekeeping parameters, and 162 engineering housekeeping parameters. Added to this information are all of the derived geometric and spatial parameters, which include spacecraft location, altitude above the asteroid surface, instrument-pointing vector, asteroid solid angle, the portion of the asteroid in the field of view, the portion of the asteroid that is illuminated, and solar angles of incidence and emission. Finally, because the asteroid surface may be highly irregular, it is possible that regions of the surface that might otherwise be illuminated and visible to the XRS will in fact be shadowed or occulted. All of these factors must be accounted for before spectra can be properly normalized and summed. For normal solar activity levels, it is expected that approximately three to six hours of observations may be necessary in order to obtain good counting statistics for any one region of the asteroid. This means normalizing and summing 100 or more spectra that may have been taken weeks apart and under very different observing conditions. Producing just the level 1 data products for the XRS is a monumental bookkeeping challenge. The following sections describe how corrections are made to spectral data to produce the level 1 data products. Details of the normalization process can be found in McClanahan *et al.* (1999a,b).

Gain Correction

Before spectra can be summed, the energy scale of each spectrum must be determined and adjusted to a common scale. For the three asteroid-pointing detectors this may be accomplished in two different ways. First, as described above it is possible to rotate Fe-55 calibration sources into the field of view. This will be done periodically throughout the mission. During every

24-h period of orbital operations, about 8 h will be spent with the high-gain antenna pointed at the Earth to return the previous 16 h of accumulated data. During this tracking period the asteroid will most likely not be in the field of view of the XRS, and it is therefore a natural time to conduct these calibrations. During the three years of cruise, several thousand hours of data have been collected by the XRS, and the gain has been remarkably stable. (There is an exception to this that will be discussed below.) This is largely due to the high-voltage control circuitry described above and in more detail in Goldsten *et al.* (1997). Therefore, the calibration sources will be used no more than once or twice a week during orbital operations. The location of the calibration rod can be determined from an engineering parameter (XRAY_CALIB_MOTOR_POS) whose value is 0 if the sources are in the home position and not in the field of view of any of the detectors. The value of this parameter is 75, 100, or 125 depending upon whether the Mg-filtered, unfiltered, or Al-filtered detector, respectively, is viewing the Fe-55 calibration source.

The asteroid-pointing detectors will, of course, also observe lines of known energy from the surface of the asteroid. Where counting statistics make it possible, these lines too can be used for energy calibration. While it may be necessary to sum several hours of data to obtain well-defined spectral features, this is still a useful exercise, because any significant gain changes during these times will be detected as line broadening.

The solar monitors cannot be calibrated by either of these methods, and must therefore rely on solar line flux for energy information. Solar flares have, on numerous occasions during cruise, produced X-ray lines from Fe and Ca of sufficient strength to be observed in solar monitor spectra. In addition, like the asteroid-pointing detectors, both the proportional counter solar monitor and the Si-PIN solar monitor have been extremely stable throughout cruise, so gain correction is not a serious issue.

Every level 1 data record will include the gain and zero of the four returned X-ray spectra. Since a single 100-s integration, even with the Fe-55 calibration source in the field of view, will not provide sufficient statistics for a reliable energy calibration, summing of spectra will be necessary. One to two hours of accumulation time, at a minimum, will generally be necessary. The gain and zero for these summed spectra will be plotted in a time series that will then be fitted with a polynomial function. Once this fitting function is defined over a long enough period of time to ensure no significant changes as newer data are collected, the gain and zero for each of the four spectra in every level 1 data record can be determined.

While the gain of the proportional counters has been quite stable in most circumstances, gain changes have been observed during two different operational situations: following high-voltage turn-on and after large solar particle events. These effects have been simulated in laboratory measurements and are believed to be due to space charging (Floyd *et al.* 1998). Following application of high voltage to the proportional counters (typically about 1165 V) the gain, as determined by measurements of the Fe-55 calibration sources, drops by about 4% and the normally Gaussian-shaped line peaks develop a low-energy tailing, as shown in Fig. 12. The effect is at its worst within about 24 h after high voltage is applied. The proportional counters take approximately four to six weeks to completely recover. Figure 12 shows the response of the Mg-filtered proportional counter to the Fe-55 source over a six-week period. The four plots represent a time progression following high-voltage turn-on on 17 March 1999. The progressive recovery from the space charging effect can be seen.

A similar effect was observed following a large solar particle event such as occurred in November 1997, but the time constants are somewhat different. The degradation develops much more slowly—taking about two weeks to reach its peak levels—and then recovers in about the same amount of time. The level of degradation never reaches that seen following high-voltage turn-on.

The XRS will be off during orbit insertion in February 2000. Following orbit insertion the instrument will be turned on and high voltage applied. There are no plans to remove high voltage again during the one year of orbital operations. Of course, a spacecraft safing event will remove power from all science instruments on *NEAR*. Several of these have occurred during cruise. High voltage may also be turned off because of detector safing. For this reason, in addition to simple gain corrections it will be necessary to monitor line tailing. Where tailing occurs, care must be taken in summing spectra.

A tailing parameter will be included with every level 1 data record. This parameter will be calculated as the ratio of the counts in two-channel (energy) regions of the X-ray spectrum when the Fe-55 source is in the field of view: channels 95–115 (valley) and channels 135–155 (peak), as indicated in Fig. 12. Because the Fe-55 source viewed by the Mg-filtered proportional counter is strongest, this detector will be used most often to determine tailing. Experience with cruise data has shown that all the proportional counters respond to space charging in a similar fashion. The tailing parameter is larger when low-energy tailing is greater. It may be as large as 0.6 about 24 h after high voltage is turned on. When there is no low-energy tailing present, this parameter will be close to 0.2. For the four curves in Fig. 12, the tailing parameters are 0.51, 0.42, 0.26, and 0.26 for 03_18_19, 04_01_99, 04_18_99, and 05_02_99, respectively. The tailing parameters at four weeks (04_18_99) and six weeks (05_02_99) are the same. This indicates that the low-energy tailing is gone, but there is still a residual effect. At four weeks after high-voltage turn-on, the peak of the Fe-55 line is located about two channels lower than where it ultimately ends up two weeks later. Also, the energy resolution has not yet returned to its nominal value of 824 eV. The Fe-55 Kα peak is broadened by about 15%.

One other issue regarding the solar monitor detectors should be mentioned. The Si-PIN detector has failed briefly on several occasions, usually following intense solar activity. Based on laboratory tests, it is believed that this effect is due to a charge buildup in the 200-nm silicon-dioxide surface layer of the Si-PIN that results in increased leakage current. The leakage current increases until the bias on the FET causes the preamplifier

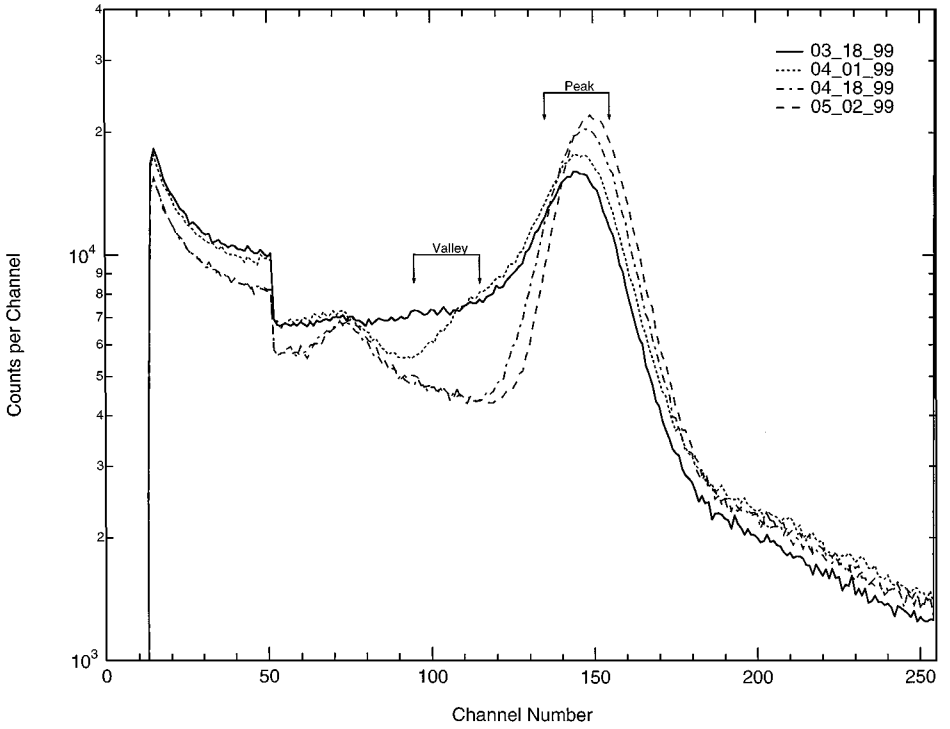

FIG. 12. Response of Mg-filtered proportional counter to Fe-55 source. The four plots represent a time progression following high-voltage turn-on on 17 March 1999. The progressive recovery from the space charging effect can be seen. The valley (channels 95–115) and peak (channels 135–155) regions used to calculate the amount of tailing are indicated.

to saturate and effectively turn off the detector (Starr *et al.* 1999). Removing high voltage from the detector for 24 to 36 h corrects this problem.

Solar Activity

Each XRS science record returns three spectra from the asteroid-pointing proportional counters and one from the active solar monitor. The active solar monitor is the detector that is pulse height analyzed during an individual integration period. This selection is made by ground command that also allows the selection of active solar monitor to alternate every integration period—a so-called "ping-pong" mode. It is this ping-pong mode that will be implemented during most orbital operations. This is a complicating factor when normalizing spectra, but each of these detectors has its advantages. The energy range of the proportional counter solar monitor is identical to that of the asteroid-pointing detectors. The proportional counters can all measure down to about 0.6 keV, while the lower level discriminator on the PIN is set at about 1.5 keV because of electronic noise. On the other hand the energy resolution of the PIN is superior to that of the proportional counters—600 and 824 eV, respectively, at 5.9 keV—which simplifies solar modeling. Also, the PIN is not subject to the same resolution degradation described above for the proportional counters.

A constant quiescent Sun throughout orbital operations would greatly simplify analysis of XRS data, but an active Sun can produce orders of magnitude more X-rays for minutes and sometimes hours, thus greatly improving counting statistics and science return for the XRS. In order to take into account large changes in solar activity for normalization of asteroid spectra, 10 levels of solar activity, labeled 0 through 9, have been defined depending on count rate in the solar monitor detectors. The definitions are different for each of the two detectors, taking into account their different response as described in Table I. The 10 levels of solar activity have been defined so that within these ranges there is little change in the slope of the solar spectrum. This allows simple summing of asteroid spectra collected while the solar X-ray input is within the same intensity level. Summing of asteroid spectra collected while solar X-ray input varies more widely requires corrections for the changing shape of the solar spectrum. This is accomplished by solar modeling which takes into account changes in effective temperature, emission measure, and X-ray line contributions at various solar levels. This process is discussed in some detail by Clark and Trombka (1997). A separate summation is made of asteroid spectra collected while the gas proportional counter is active as opposed to the Si-PIN detector. While the two solar monitors have been intercalibrated, the summed spectra normalized by the two different solar monitors are not summed at level one processing.

Solar Angles of Incidence and Emission, Shadowing, and Occultation

The XRS experiment is not possible without the solar X-rays that excite the atoms in the surface of the asteroid, but even with

TABLE I
Solar Level Definitions for Si-PIN and Proportional Counter Solar Monitors

Solar level	Si-PIN Detector	Proportional counter
0	$0 < SL < 3{,}500$	$0 < SL < 16{,}000$
1	$3{,}500 \le SL < 5{,}000$	$16{,}000 \le SL < 32{,}000$
2	$5{,}000 \le SL < 7{,}000$	$32{,}000 \le SL < 63{,}000$
3	$7{,}000 \le SL < 11{,}000$	$63{,}000 \le SL < 100{,}000$
4	$11{,}000 \le SL < 20{,}000$	$100{,}000 \le SL < 105{,}000$
5	$20{,}000 \le SL < 40{,}000$	$105{,}000 \le SL < 120{,}000$
6	$40{,}000 \le SL < 80{,}000$	$120{,}000 \le SL < 140{,}000$
7	$80{,}000 \le SL < 200{,}000$	$140{,}000 \le SL < 180{,}000$
8	$200{,}000 \le SL < 1{,}750{,}000$	$180{,}000 \le SL < 1{,}900{,}000$
9	$1{,}750{,}000 \le SL$	$1{,}900{,}000 \le SL$

Note.

$$SL = 300 \sum_{i}^{256} Solar\_Spectrum(\mathrm{I}) \times \frac{Sun\_Distance^2}{Cos\_Angle\_Sol\_Mon \cdot Solar\_Live\_Time \cdot Actv\_Sol\_Mon\_Integ\_Time \cdot D_0^2}$$

where $i = 32$ for PIN, 19 for Gas and $D_0 = 1.4AU$

constant solar flux other solar-related issues need to be accounted for when normalizing spectra. Both the angle of incidence between the Sun and the asteroid surface (α) and the angle of emission between the asteroid surface and the detector boresite (β) will vary. Both of these angles are defined with respect to the normal to the asteroid surface so small angles or large angle cosines are preferred. These angles are important not only for geometric normalization, but are also part of the mass absorption correction as described by Clark and Trombka (1997). When the product of cosine(α)*cosine(β) is less than 0.25, data are excluded from routine summations.

A detailed shape model of Eros will be used to define all geometric and spatial parameters including angles of incidence and emission. Naturally this model may change as more imaging and laser altimetry data become available. Two important issues in this regard are shadowing and occultation. In shadowing, a portion of the asteroid that would normally be illuminated by the Sun is in darkness because another feature of the asteroid is shading it. X-ray data collected from a region that contains such a case would not provide any information on the shaded region, and factors such as effective area of the surface being sampled must be corrected. Occultation presents a similar problem to shadowing. In this case a region that is illuminated and nominally in the XRS field of view cannot be observed because another surface feature is in the line of site of the XRS. Again corrections to effective area must be made.

Spatial and Geometric Factors

Proper normalization of X-ray spectra requires careful attention to a number of geometric and spatial factors. An important part of this normalization procedure is the representation of the asteroid shape as a virtual surface made up of triangular plates. The plate model that the XRS will use to describe the size and shape of Eros is made up of 8200 plates, each about 0.5 to 1.0 km on a side. Superimposed on this plate model is a bin model that sums plates into near equal area spatial units. The bin size is chosen based on the spatial resolution of the instrument—a little bit less than the size of the footprint at 50 km, or about 3 km in diameter. Bins, therefore, include about 8 to 10 plates.

As mentioned above, the MET provides a link to the SPICE kernels that provide Sun, Earth, and spacecraft position. Combining this information with the plate model allows, for each science record, calculation of instrument boresight, average incidence and emission angles, footprint area, total illuminated area, total visible area, total effective area, and total effective solid angle. Each level 1 science data product will include all of these derived parameters.

A field-of-view status flag (`FOV_status`) will also be attached to every record. Its purpose is to describe the applicability of the level 1 science record to different science and mission planning activities. A set of five possible values has been specified for each level 1 science record as described in Table II. Category 0 data will be used for cosmic background measurements. Categories 2 and 4 will be used for asteroid background determination. Categories 1 and 3 will be used for processing fluorescence spectral data.

Bad Data Records

As described above, the DQI is 0 if all of the data packets for a science record have been received and 1 if any packets are missing. In addition, team members review all data records received by the SDC to scan for "bad data" records. Examples of bad data are those records with corrupted spectral or housekeeping data due to transmission problems, where one or more detectors have entered safing mode, when high voltage is outside of the nominal range, or any other anomaly that may result in a degraded summed spectrum. A bad data flag is included with each record; it is zero if data may be used without reservation, and one if data are suspect. Brief explanations for bad data flags are also included.

LEVEL 2 DATA PRODUCTS

The *NEAR* XRS level 2 data products are summed spectra and peak areas extracted from the summed spectra for the X-ray

TABLE II
XRS Field-of-View Status

FOV_status	XRS field of view
0	Completely off the asteroid
1	Completely filled by the asteroid and at least part of the footprint is illuminated
2	Completely filled by the asteroid and is completely dark
3	Partially filled by the asteroid and at least part of the footprint is illuminated
4	Partially filled by the asteroid and is completely dark

lines of interest. These summed spectra include all of the normalization factors described above for the level 0 and level 1 data products. The number of spatial units (bins) will vary with time. Early in the mission only global results will be possible; the number of bins is just 1. As the *NEAR* mission progresses and more data are collected, the result will be improved statistics for previously defined bins or, if statistics permit, rebinning of the asteroid surface that will provide finer spatial resolution.

Peak Area Extraction above 2 keV

Above 2 keV, the X-ray lines that are of interest for geochemical purposes are Ca (3.692 keV), Ti (4.511 keV), and Fe (6.404 keV). The first step in extracting these peak areas is to identify the background. The cosmic-ray background component can be determined from XRS measurements collected when neither the asteroid nor any sky X-ray sources are in the field of view (`FOV_status = 0`). Measurements of the dark side of the asteroid will contain coherent scattering of sky X-ray sources from the surface as well as a contribution from cosmic rays (`FOV_status = 2, 4`).

Peak area extraction is accomplished by fitting peaks and background simultaneously. Background may be subtracted first, leaving just the peaks for fitting, but generally speaking, fitting the background and the peaks at the same time will produce more reliable results. The fitting procedure uses the previously determined background shape and intensity and the response function of the proportional counters at the appropriate energies. Many fitting methods are available, and in most cases different methods will be used on the same spectra to confirm the analysis. The spectra from all three asteroid-pointing proportional counters can be summed to enhance the signals from the Ca, Ti, and Fe lines.

Peak Area Extraction below 2 keV

Below 2 keV, the X-ray lines of interest for geochemical purposes are Mg (1.254 keV), Al (1.487 keV), and Si (1.740 keV). Analysis of these three X-ray lines is complicated by the fact that they cannot be separately resolved by the proportional counters. The energy resolution of the proportional counters at these energies is nearly 30%, far too great to observe any separation of these lines. This is the reason for including the Mg and Al filters. The sharp K-edges of these two filters preferentially allow different amounts of the three X-ray lines to be detected by the Mg- and Al-filtered detectors. The response of these two detectors and the unfiltered detector are identical, except for these filters. Combining the spectral measurements from the two filtered detectors with that of the unfiltered detector makes the extraction of peak areas possible. The problem reduces to one of matrix inversion or solution of simultaneous equations—three equations and three unknowns.

If N is the number of counts in each of the three detectors in the energy region 1 to 2 keV, S is the signal from the asteroid, B

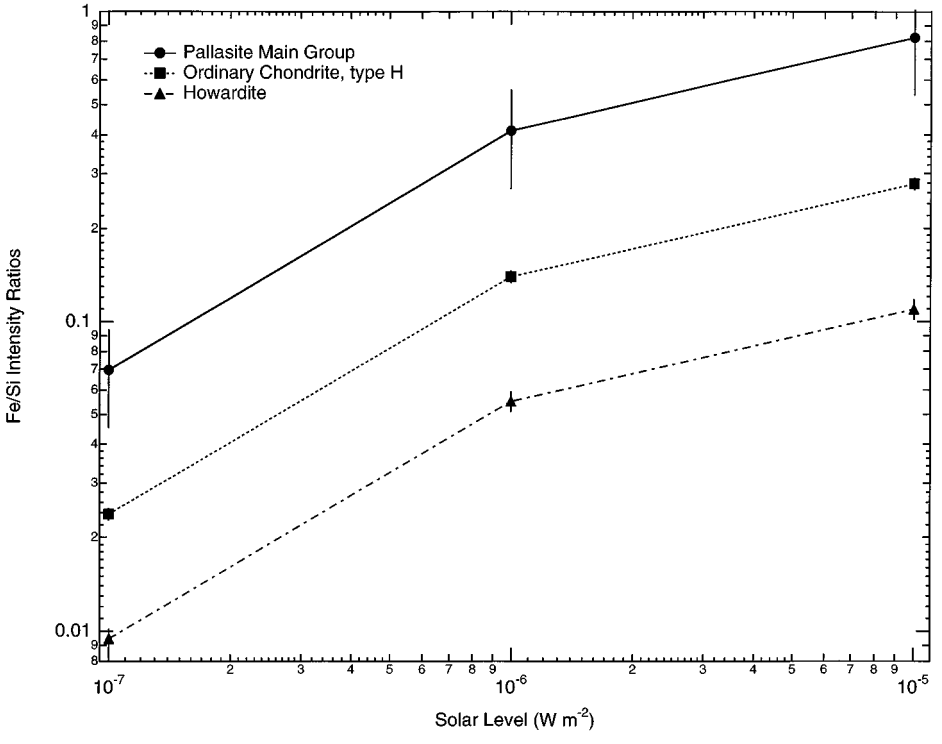

FIG. 13. Fe/Si intensity ratios versus solar activity level for three different meteorite classes. Solar levels are B1, 10^{-7} Wm^{-2}; C1, 10^{-6} Wm^{-2}; and M1, 10^{-5} Wm^{-2}.

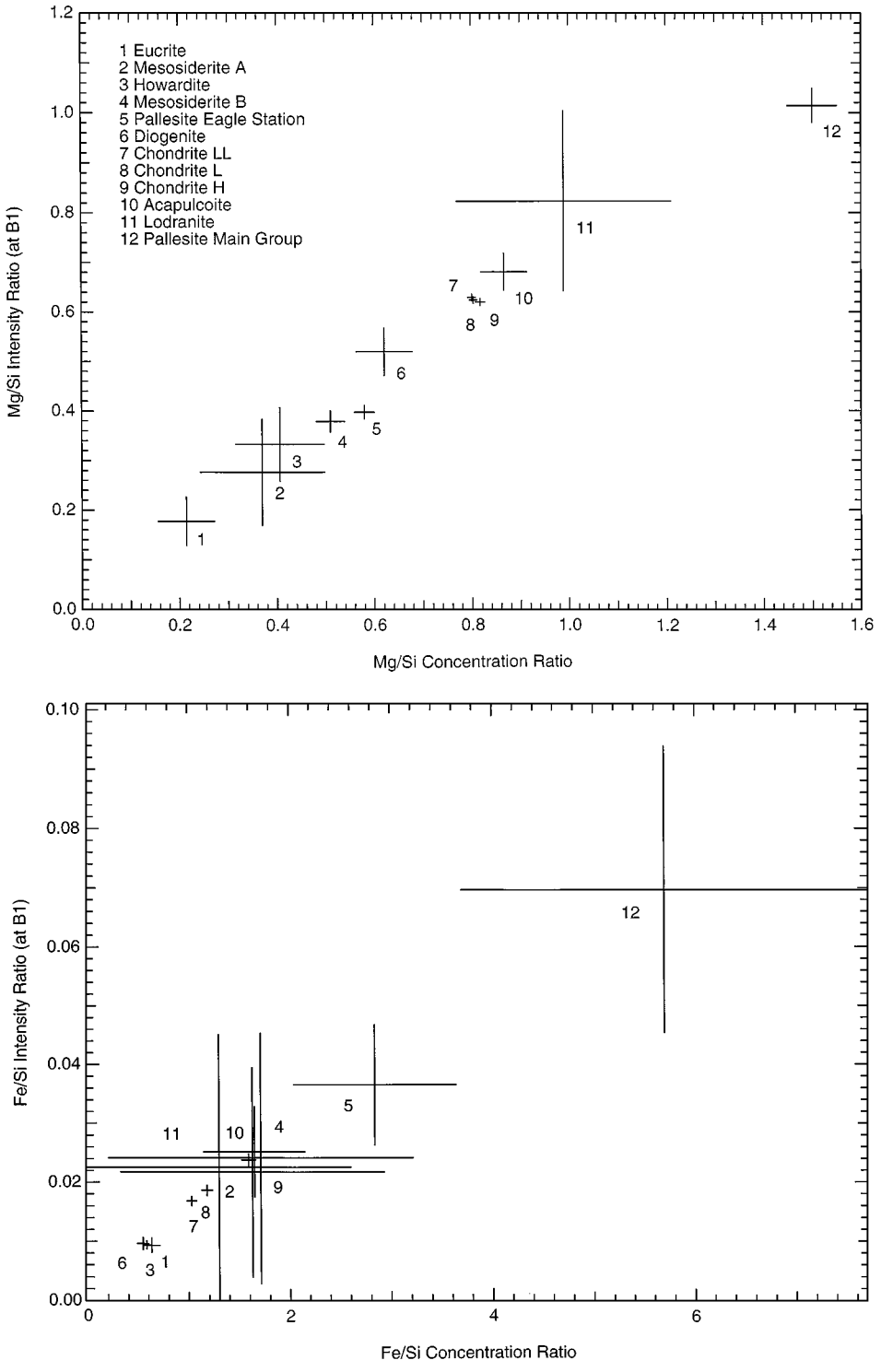

FIG. 14. Mg/Si (top) and Fe/Si (bottom) intensity ratios (for B1 solar activity level) versus concentration ratios for 12 different meteorite classes.

is the background, and f is the filter factor (detector efficiency at the specified energy), we then have

Unfiltered detector:

$$N_{\mathrm{unf}} = f_{\mathrm{unfSi}} S_{\mathrm{Si}} + f_{\mathrm{unfAl}} S_{\mathrm{Al}} + f_{\mathrm{unfMg}} S_{\mathrm{Mg}} + B_{\mathrm{unf}},$$

Mg-filtered ditector:

$$N_{\mathrm{Mg}} = f_{\mathrm{MgSi}} S_{\mathrm{Si}} + f_{\mathrm{MgAl}} S_{\mathrm{Al}} + f_{\mathrm{MgMg}} S_{\mathrm{Mg}} + B_{\mathrm{Mg}},$$

Al-filtered detector:

$$N_{\mathrm{Al}} = f_{\mathrm{AlSi}} S_{\mathrm{Si}} + f_{\mathrm{AlAl}} S_{\mathrm{Al}} + f_{\mathrm{AlMg}} S_{\mathrm{Mg}} + B_{\mathrm{Al}}.$$

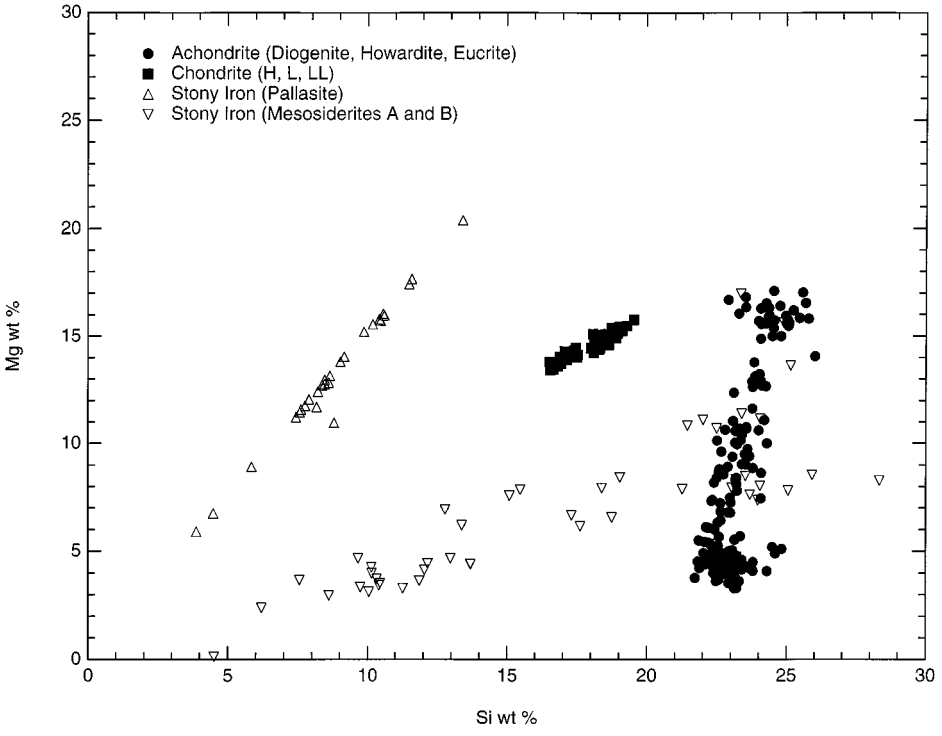

FIG. 15. Mg concentration versus Si concentration for different meteorite classes. Very distinct patterns can be seen for achondrite, chondrite, and two different subclasses of stony iron.

Solving the above set of simultaneous equations for the three unknowns, S_{unf}, S_{Mg}, and S_{Al} is straightforward. Table III gives the nine filter factors. Those for the unfiltered detector are calculated. The actual filter thicknesses have been determined by X-ray transmission measurements, and they are 9.2 and 9.0 μm for the Mg and Al filters, respectively.

LEVEL 3 DATA PRODUCTS

The level 3 data products are the final results of the XRS analysis. They will include line intensity ratios, elemental concentrations, and classification(s) with known meteorite group(s). A detailed description of the method for calculating the X-ray fluorescence for the Kα line for each element, as well as the coherent and incoherent scatter in the vicinity of the line, is given in Clark and Trombka (1997). Using the parameters and equations described in Clark and Trombka (1997) along with the geometric factors and normalizations described here in previous sections, elemental abundances can be calculated from the XRS spectra. Beyond this basic step, however, using line ratios and relating these ratios to various meteorite compositions can confirm the abundance calculations and is a powerful technique for evaluating the XRS data.

TABLE III
Detector Filter Factors

Detector	Si line	Al line	Mg line
Unfiltered	0.600	0.439	0.264
Mg filtered	0.008	0.001	0.116
Al filtered	0.000	0.165	0.059

Line Intensity Ratios and Elemental Concentrations

Line intensity ratios are a valuable analysis tool, especially in the early stages of XRS investigations. Matrix effects that could result from gross physical and compositional variations in the regolith are significantly reduced and most of the geometric corrections described above also cancel out.

Models of surface X-ray spectra production have been developed in order to generate theoretical spectra for a variety of targets and to predict the relationship between elemental line intensity ratios and concentration ratios under anticipated solar conditions. These models must take into consideration not only the anticipated solar flux, but also the anticipated range of elemental concentrations in the target. Line intensity ratios at a particular level of solar output will show the same relationship as long as the slope of the solar spectrum has been correctly modeled for a given level of solar activity. This is true even if the integrated solar flux is not measured with absolute accuracy. Figure 13 shows calculated Fe/Si line intensity ratios as a function of solar flux for three different classes of meteorites. These predicted intensity ratios can be compared to measured intensity

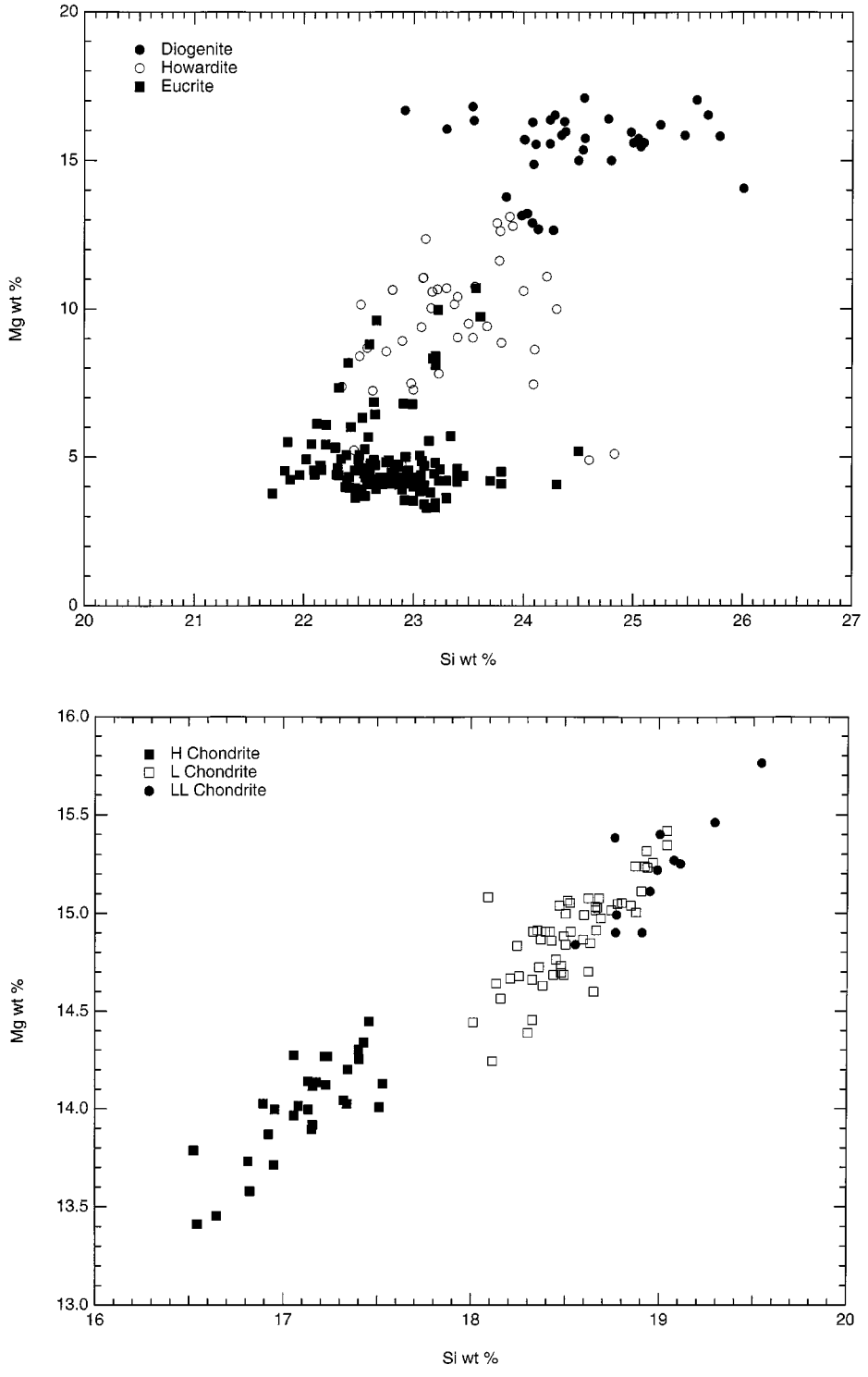

FIG. 16. Mg versus Si concentrations for achondrites (top) and chondrites (bottom). Separation of various subclasses can be seen.

ratios obtained for the same area on Eros, but at different times in order to verify the normalization for solar variation. Of the various line ratios measurable by the XRS, the Fe/Si ratio is the most sensitive to changes in solar flux because these two X-ray lines are widely separated in energy. As the solar spectrum hardens during larger flares the intensity of the higher energy Fe line increases relative to the lower energy Si line.

Unlike the Apollo XRS experiments from the Moon, ground truth samples will not be available from Eros. Instead, initial measurements of its bulk composition will be used to try to

relate Eros to a particular meteorite class. Figure 14 shows plots of Mg/Si intensity ratios versus Mg/Si concentration ratios and Fe/Si intensity ratios versus Fe/Si concentration ratios for several meteorite classes, calculated assuming a B1 solar level. Error bars indicate the 1σ standard deviation observed in laboratory analyses of different meteorites of a given type. Such plots will be used to determine a likely meteorite analog for Eros. By using several such plots of different element ratios, meteorite class and in some cases even meteorite subclass may be reliably established.

Surface maps of line intensity ratios will reflect changes in surface chemistry. Line ratio maps made with respect to a constant abundance element preserve a direct relationship between the ratio data and the abundance data for the variable element. If preliminary measurements indicate that Eros most closely resembles, for example, a basaltic achondrite, where Si abundances do not vary significantly with subclass, then surface maps of line intensity ratios with respect to Si may be generated. If Eros more closely resembles a stony-iron meteorite where Si concentrations can vary significantly depending on the relative amount of metal and silicate locally present, then surface maps of line ratios with respect to Si are less easily interpreted, but still useful. In either case, these maps represent an intermediate step. Ultimately, the goal of the XRS measurements is to develop surface maps of absolute concentrations for the various major elements, but the ratio maps should provide useful consistency checks on elemental abundance calculations.

Comparison of various elemental concentrations will probably be the most sensitive way to distinguish between the various possible meteorite class analogs of Eros and to identify particular geological processes that have occurred on the asteroid. Figure 15 displays a plot of Mg concentration versus Si concentration generated from a large library of meteorite laboratory measurements compiled and organized by the XRS team. Distinct patterns can be seen for HED achondrites, ordinary chondrites, and two different classes of stony irons. Figure 16 shows data for just the achondrites and chondrites where separation of subclasses can be clearly seen. Comparing measured abundances of the asteroid to this library of meteorite composition data should permit us to associate Eros with both meteorite class and subclass.

Comparisons with Other NEAR Instruments

XRS results will be enhanced by comparisons with observations from other *NEAR* instruments. The extent of surface heterogeneity on a scale of kilometers to tens of kilometers and, by implication, the degree of differentiation and the nature of processes in the early Solar System can be determined by the XRS experiment. Correlation of XRS measurements with observations from the multi-spectral imager (surface expression of geochemical terrains), the *NEAR* infrared spectrometer (mineralogy), the *NEAR* laser ranger (vertical extent of terrains), and the magnetometer (orientation during formation) will further the characterization of these heterogeneities.

The depth and extent of dust cover on asteroids is a controversial issue. Differences between Fe data, derived from the XRS and gamma-ray spectrometer experiments, should be due to differences in near-surface stratigraphy, and could put constraints on the thickness of a surface dust layer. Fluorescent X-rays are generated at the very surface (in the top $\ll 1$ mm), whereas gamma rays are generated at depths of 10 to 20 cm. When spatial resolutions for the two results are made comparable, any differences in Fe concentration measurements could be the result of differences in the composition of the top layer of the asteroid.

ACKNOWLEDGMENTS

The authors thank the *NEAR* mission operations team at the Johns Hopkins Applied Physics Laboratory whose cooperation and support along with that of the program manager, T. B. Coughlin, and Project Scientist, A. F. Cheng, have made possible the collection of thousands of hours of cruise data.

REFERENCES

Adler, I., J. Gerard, J. I. Trombka, R. Schmadebeck, P. Lowman, H. Blodgett, L. Yin, E. Eller, and R. Lamothe 1972b. The Apollo 15 X-ray fluorescence experiment. *Proc. Lunar Sci Conf. 3rd*, 2157–2178.

Adler, I., J. I. Trombka, J. Gerard, P. Lowman, R. Schmadebeck, H. Blodgett, E. Eller, L. Yin, R. Lamothe, P. Gorenstein, and P. Bjorkholm 1972a. Apollo 15 geochemical X-ray fluorescence experiment: Preliminary report. *Science* **175**, 436–440.

Adler, I., J. I. Trombka, J. Gerard, P. Lowman, R. Schmadebeck, H. Blodgett, E. Eller, L. Yin, R. Lamothe, G. Osswald, P. Gorenstein, P. Bjorkholm, H. Gursky, and B. Harris 1972c. Apollo 16 geochemical X-ray fluorescence experiment: Preliminary report. *Science* **177**, 256–259.

Clark, P. E. 1979. *Composition of Theoretically Calculated and Observed XRF Data Intensity Ratios.* Ph.D. Dissertation, University of Maryland, College Park, MD.

Clark, P. E., and J. I. Trombka 1997. Remote X-ray spectrometry for NEAR and future missions: Modeling and analyzing X-ray production from source to surface. *J. Geophys. Res.* **102**, 16,361–16,384.

Clark, P. E., J. I. Trombka, and S. Floyd 1995. Solar monitor design for the NEAR X-ray spectrometer, *Lunar Planet. Sci.* **26**, 253–254.

Floyd, S. R., J. I. Trombka, P. E. Clark, R. Starr, H. W. Leidecker, J. O. Goldsten, and D. R. Roth 1998. Radiation effects on the proportional counter X-ray detectors on board the NEAR spacecraft. *Nucl. Inst. Meth. Phys. Res. A* **422**, 577–581.

Goldsten, J. O., R. L. McNutt, Jr., R. E. Gold, S. A. Gary, E. Fiore, S. E. Schneider, J. R. Hayes, J. I. Trombka, S. R. Floyd, W. V. Boynton, S. Bailey, J. Brückner, S. W. Squyres, L. G. Evans, P. E. Clark, and R. Starr 1997. The X-ray/gamma-ray spectrometer on the Near Earth Asteroid Rendezvous mission. *Space Sci. Rev.* **82**, 169–216.

Knoll, G. F. 1989. *Radiation Detection and Measurement*, Chap. 6 Wiley, New York.

McClanahan, T. P., I. Mikheeva, J. I. Trombka, S. R. Floyd, W. V. Boynton, H. Bailey, J. Bhangoo, R. Starr, P. E. Clark, L. G. Evans, S. Squyres, E. McCartney, E. Noe, R. McNutt, and J. Brückner 1999b. Data processing for the Near Earth Asteroid Rendezvous (NEAR) X-ray and gamma-ray spectrometer (XGRS) ground system. In *Proc. of SPIE* (R. B. James and R. C. Schirato, Eds.), Vol. 3768, SPIE, pp. 74–87.

McClanahan, T. P., J. I. Trombka, S. R. Floyd, W. V. Boynton, I. Mikheeva, H. Bailey, C. Liewicki, J. Bhangoo, R. Starr, P. E. Clark, L. G. Evans, S. Squyres, R. McNutt, and J. Brückner 1999a Data management and

analysis techniques used in the NEAR X-ray and gamma-ray spectrometer systems. *Nucl. Inst. Meth. Phys. Res. A* **422**, 582–585.

Starr , R., P. E. Clark, L. G. Evans, S. R. Floyd, T. P. McClanahan, J. I. Trombka, J. O. Goldsten, R. H. Maurer, R. L. McNutt, Jr., and D. R. Roth 1999. Radiation effects in the Si-PIN detector on the Near Earth Asteroid Rendezvous Mission. *Nucl. Inst. Meth. Phys. Res. A* **428**, 209–215.

Trombka, J. I., W. V. Boynton, J. Brückner, S. W. Squyres, P. E. Clark, R. Starr, L. G. Evans, S. R. Floyd, E. Fiore, R. E. Gold, J. O. Goldsten, R. L. McNutt, Jr., and S. H. Bailey 1997. Compositional mapping with the NEAR X-ray/gamma-ray spectrometer. *J. Geophys. Res.* **102**, 23,729–23,750.

Trombka, J. I., R. L. Schmadebeck, M. J. Bielefeld, L. G. Evans, A. E. Metzger, E. L. Haines, C. S. Dyer, S. M. Seltzer, R. C. Reedy, and J. R. Arnold 1979. Analytical methods in determining elemental composition from the Apollo X-ray and gamma-ray spectrometer data. In *Computers in Activation Analysis and Gamma-ray Spectroscopy* (B. S. Carpenter, M. D'Agostino,and H. Yule, Eds.), pp. 26–38. Nat. Tech. Inf. Service., U.S. Dept. of Commerce, Springfield, VA.

Veverka, J., J. F. Bell III, P. Thomas, A. Harch, S. Murchie, S. E. Hawkins, Jr., J. W. Warren, H. Darlington, K. Peacock, C. R. Chapman, L. A. McFadden, M. C. Malin, and M. S. Robinson 1997. An overview of the NEAR multispectral imager-near-infrared spectrometer investigation. *J. Geophys. Res.* **102**, 23,709–23,728.

Yin, L. I., J. I. Trombka, I. Adler, and M. Bielefeld 1993. X-ray remote sensing techniques for geochemical analysis of planetary surfaces. In *Remote Geochemical Analysis: Elemental and Mineralogical Composition*, (C. Pieters and P. Englert Eds.), pp. 199–212. Cambridge Univ. Press, Cambridge, UK.

Zuber, M. T., D. E. Smith, A. F. Cheng, and T. D. Cole 1997. The NEAR laser ranging investigation, *J. Geophys. Res.* **102**, 23,761–23,774.